



Reductive Transformation of Layered-Double-Hydroxide Nanosheets to Fe-Based Heterostructures for Efficient Visible-Light Photocatalytic Hydrogenation of CO

Yufei Zhao, Zhenhua Li, Mengzhu Li, Jinjia Liu, Xingwu Liu, Geoffrey I. N. Waterhouse, Yuanshen Wang, Jiaqing Zhao, Wa Gao, Zhaosheng Zhang, Run Long, Qinghua Zhang, Lin Gu, Xi Liu, Xiaodong Wen, Ding Ma,* Li-Zhu Wu, Chen-Ho Tung, and Tierui Zhang**

Conversion of syngas (CO, H_2) to hydrocarbons, commonly known as the Fischer-Tropsch (FT) synthesis, represents a fundamental pillar in today's chemical industry and is typically carried out under technically demanding conditions (1–3 MPa, 300–400 °C). Photocatalysis using sunlight offers an alternative and potentially more sustainable approach for the transformation of small molecules ($\text{H}_2\text{O}, \text{CO}, \text{CO}_2, \text{N}_2$, etc.) to high-value products, including hydrocarbons. Herein, a novel series of Fe-based heterostructured photocatalysts (Fe-x) is successfully fabricated via H_2 reduction of ZnFeAl -layered double hydroxide (LDH) nanosheets at temperatures (x) in the range 300–650 °C. At a reduction temperature of 500 °C, the heterostructured photocatalyst formed (Fe-500) consists of Fe^0 and FeO_x nanoparticles supported by ZnO and amorphous Al_2O_3 . Fe-500 demonstrates remarkable CO hydrogenation performance with very high initial selectivities toward hydrocarbons (89%) and especially light olefins (42%), and a very low selectivity towards CO_2 (11%). The intimate and abundant interfacial contacts between metallic Fe^0 and FeO_x in the Fe-500 photocatalyst underpins its outstanding photocatalytic performance. The photocatalytic production of high-value light olefins with suppressed CO_2 selectivity from CO hydrogenation is demonstrated here.

Light olefins ($\text{C}_2\text{--C}_4$) are a key building block of today's chemical industry and widely used for synthesis of polymers, drugs, and other speciality chemicals. Generally, light olefins are synthesized by the hydrogenation of CO through the Fischer-Tropsch (FT) reaction^[1] or from methanol.^[2] Although high selectivities to olefins can be achieved using bifunctional catalysts that allow the stepwise transformation of syngas ($\text{CO} + \text{H}_2$) to methanol and then methanol to light olefins at 1–3 MPa and temperatures above 400 °C, a one-step process from syngas to olefins under milder reaction conditions is highly desirable. The development of such an alternative one-step CO hydrogenation process to light olefins has proved very challenging, due to the need for precise catalyst control of the extent of hydrogenation of surface intermediates such as

Dr. Y. Zhao, Z. Li, Y. Wang, J. Zhao, Prof. L.-Z. Wu, Prof. C.-H. Tung,
Prof. T. Zhang

Key Laboratory of Photochemical Conversion
and Optoelectronic Materials
Technical Institute of Physics and Chemistry
Chinese Academy of Sciences
Beijing 100190, China
E-mail: tierui@mail.ipc.ac.cn

Z. Li, Y. Wang, J. Zhao
Key Laboratory of Synthetic and Natural Functional
Molecule Chemistry of the Ministry of Education
College of Chemistry & Materials Science
Northwest University
Xi'an 710127, China

M. Li, Dr. W. Gao, Prof. D. Ma
College of Chemistry and Molecular Engineering
and College of Engineering
BIC-ESAT, Peking University
Beijing 100871, China
E-mail: dma@pku.edu.cn

J. Liu, Dr. X. Liu, Prof. X. Liu, Prof. X. Wen
State Key Laboratory of Coal Conversion
Institute of Coal Chemistry
Chinese Academy of Sciences
Taiyuan 030001, China
E-mail: wxd@sxicc.ac.cn

J. Liu, Dr. X. Liu, Prof. X. Liu, Prof. X. Wen
Synfuels China

Beijing 100195, China
Prof. G. I. N. Waterhouse
School of Chemical Sciences
The University of Auckland
Auckland 1142, New Zealand

Z. Zhang, Prof. R. Long
College of Chemistry
Key Laboratory of Theoretical and Computational
Photochemistry of Ministry of Education
Beijing Normal University
Beijing 100875, China

Dr. Q. Zhang, Prof. L. Gu
Beijing National Laboratory for Condensed Matter Physics
Institute of Physics
Chinese Academy of Sciences
Beijing 100190, China

Prof. T. Zhang
University of Chinese Academy of Sciences
Beijing 100049, China

The ORCID identification number(s) for the author(s) of this article
can be found under <https://doi.org/10.1002/adma.201803127>.

DOI: 10.1002/adma.201803127

$-\text{CH}_2$ species (to prevent CH_4 formation and to promote C–C coupling reactions), and also the need to suppress the water gas shift (WGS) reaction that leads to undesirable CO_2 evolution.^[3]

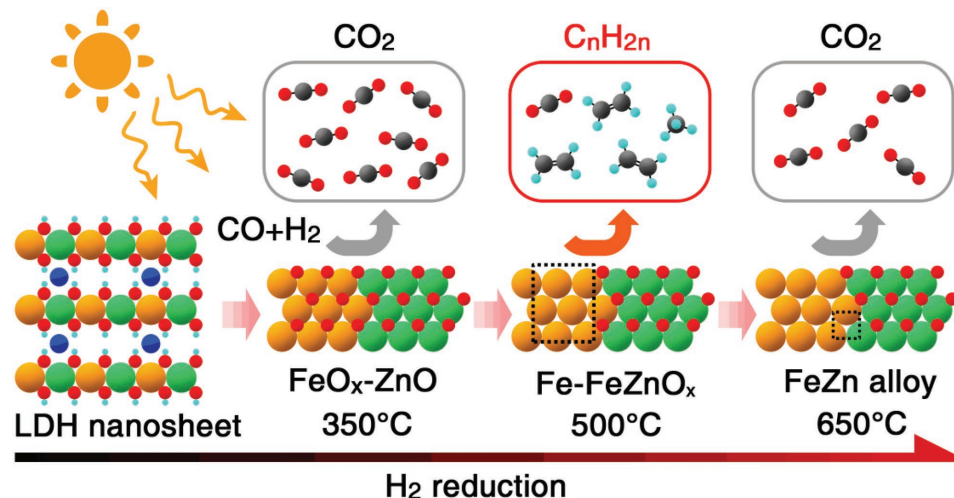
Semiconductor photocatalysis offers enormous potential for transforming abundant solar energy into fuels and valuable chemical feedstocks via processes such as water splitting, CO_2 reduction, and N_2 fixation.^[4] In recent work, we demonstrated that alumina supported NiO/Ni nanostructures formed by the reduction of NiAl -layered double hydroxide (LDH) nanosheets previously calcined at 400–600 °C were active for both CO activation and C–C coupling reactions under visible excitation. In particular, the alumina supported NiO/Ni photocatalysts exhibited high selectivity for the synthesis of C_{2+} hydrocarbons (mainly C_2 – C_6 alkanes) from syngas.^[5] The high selectivity to alkanes reflected the very strong hydrogenation ability of Ni-containing photocatalysts. Potentially the same synthetic strategy could be adopted for the synthesis of photocatalysts with high selectivities for CO hydrogenation to olefins, by replacing Ni in the LDH nanosheet precursor with metal cations of milder hydrogenation ability.^[6] It is well understood that during the FT reaction, CO hydrogenation to olefins generally follows a volcano curve, wherein the binding energy of key intermediates (like $-\text{CH}_2$ and its coupling products) should not be too strong; otherwise the hydrogenation to the alkane will occur.^[7] Compared with Ni and Co-containing catalysts,^[1b,8] Fe-based catalysts offer far more moderate intermediate binding energies on account of their unique electronic structure, suggesting that an Fe-based photocatalyst system might afford a highly selective pathway of olefins during CO hydrogenation. To date, no study has reported the successful development of earth-abundant photocatalysts for the transformation of CO to light olefins, motivating an in-depth investigation.

Herein, inspired by the aforementioned considerations, we describe the successful synthesis of a series of Fe- x photocatalysts by hydrogen reduction of a ZnFeAl-LDH nanosheet precursor at different temperatures (x) (**Scheme 1**). At reduction temperatures above 400 °C, partial reduction of iron occurred to give Fe- x photocatalysts comprising Fe^0 , and

FeO_x supported on ZnO-alumina. An Fe-500 photocatalyst showed remarkable performance for photocatalytic FT reaction under UV-vis excitation, affording a very high selectivity to olefins ($\approx 43\%$ C_2 – C_4 olefins vs $\approx 9\%$ C_2 – C_4 paraffins) and a very low selectivity to CO_2 ($\approx 11\%$) under batch or flow reactor tests. The hydrogenation performance of metallic Fe in Fe-500 was modulated favorably by FeO_x and the ZnO-alumina mixed oxide support, allowing precise tuning of the CO hydrogenation product high selectivity towards light olefins and suppressed CO_2 formation. Results pave the way for the development of other novel photocatalyst systems for solar-driven FT reactions.

LDH precursors were reported to afford exceptional advantages for the synthesis of monodisperse supported Ni and Fe nanoparticles for the growth of carbon nanotubes, as was first reported by the Li^[9] and Wei groups.^[10] Accordingly, a ZnFeAl-LDH nanosheet precursor was chosen here for the synthesis of the Fe-based FT photocatalysts, the justification for which was as follows. Zinc oxide is an excellent semiconductor and structural promoter for iron species, ensuring small Fe particle sizes and thus improved FT activity,^[11] whereas Al_2O_3 is a thermally stable support that is beneficial for avoiding undesirable catalyst sintering and aggregation during reaction.

Figures S2 and S3A (Supporting Information) confirm the successful synthesis of ZnFeAl-LDH nanosheets, with the desired Zn:Fe:Al molar ratio (1:1:1) and a nanosheet size of ≈ 50 nm and thickness 2.1 nm. The ultrathin nanosheets allow the topological transformation to highly dispersed metal/support catalysts with heating in a reducing atmosphere. X-ray diffraction (XRD) was used to track the H_2 reduction process of the ZnFeAl-LDH nanosheet precursor at temperatures between 300 and 650 °C (the obtained samples are denoted as Fe- x , where x is the reduction temperature, **Figure 1A**). The XRD pattern of Fe-300 had lost the characteristic (00l) reflections of the LDH precursor, indicating that the LDH structure had collapsed completely during heating in H_2 at 300 °C for 2 h. Fe-350 showed some weak features due to the formation of Fe_2O_3 . When the reduction temperature increased above 400 °C, peaks due to metallic Fe appeared, whilst ZnO appeared above



Scheme 1. The Fe- x photocatalysts that were obtained by hydrogen reduction of ZnFeAl-LDH nanosheets at different temperatures (x), and their selectivities for CO hydrogenation under UV-vis excitation.

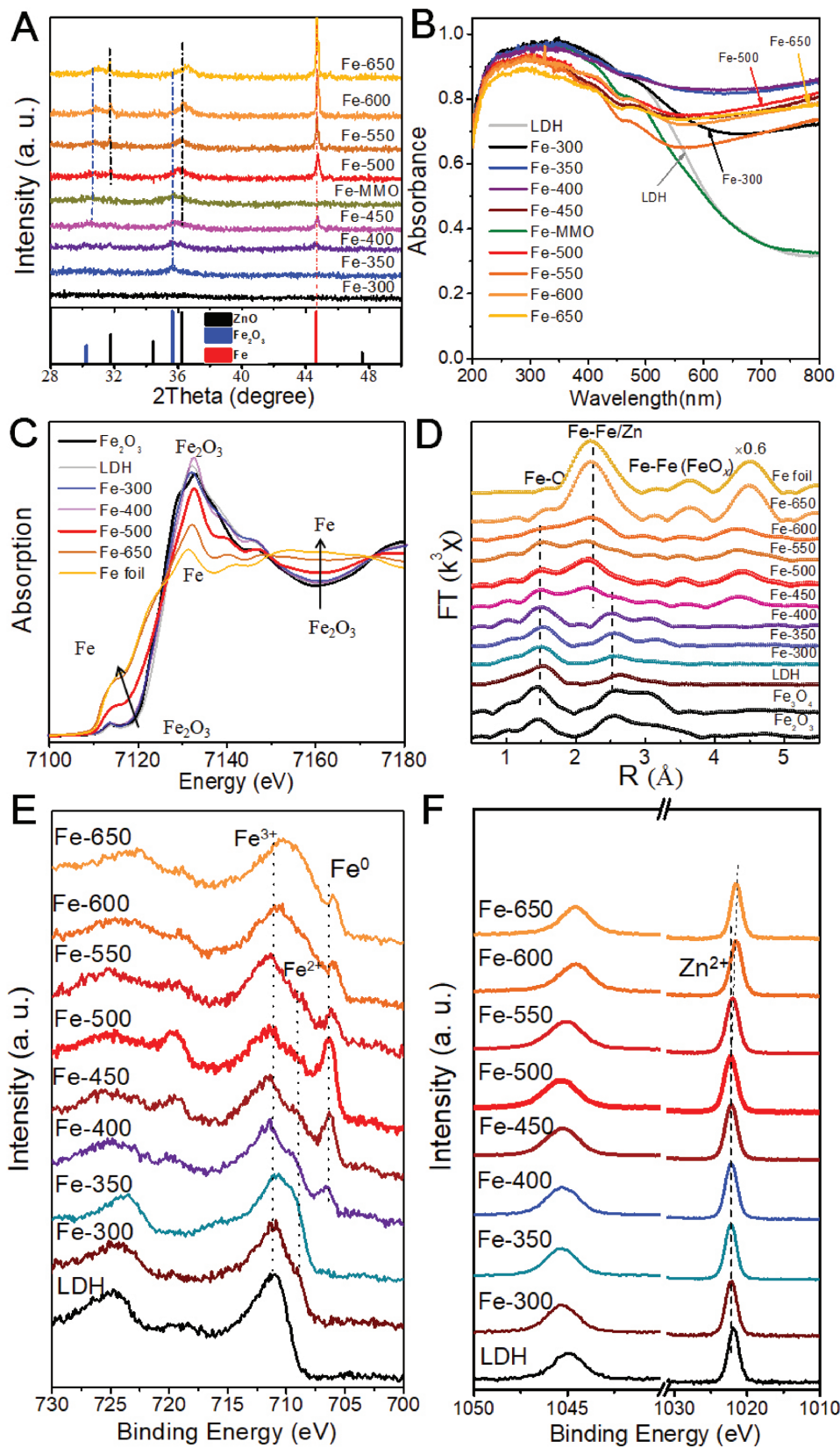


Figure 1. A) XRD patterns of Fe-x and Fe-MMO. B) UV-vis spectra of Fe-x, Fe-MMO, and ZnFeAl-LDH. C) Fe K-edge XANES and D) EXAFS spectra of Fe-x and ZnFeAl-LDH. Data for various reference compounds are also provided. E,F) In situ XPS spectra of Fe 2p (E) and Zn 2p (F) regions for Fe-x and ZnFeAl-LDH.

500 °C. The intensity of metallic Fe component increased with reduction temperature up to 650 °C. The product of calcining the ZnFeAl-LDH nanosheet precursor at 500 °C in air (denoted herein as Fe-MMO) showed signals due to ZnO and Fe₂O₃, confirming the importance of H₂ in Fe nanoparticle development in the Fe-*x* system. The absence of XRD pattern of Al₂O₃ in the Fe-*x* and Fe-MMO samples confirms an amorphous phase.

UV-vis absorption spectra were collected for the Fe-*x* photocatalysts to gauge their light absorption ability for photocatalytic applications (Figure 1B). The ZnFeAl-LDH nanosheet precursor and Fe-MMO both showed strong absorption below 500 nm due to the presence of Fe³⁺ species, whereas the Fe-*x* photocatalysts reduced above 400 °C absorbed strongly across the whole visible spectrum consistent with their black appearance (Figure S4A, Supporting Information). The increased absorption ability coincides with the evolution of metallic Fe nanoparticles.

The performance of the Fe-*x* photocatalysts for CO hydrogenation (CO/H₂/N₂ = 20/60/20, 0.18 MPa) under UV-vis irradiation was subsequently evaluated, with results summarized in Table 1. Under UV-vis excitation, ZnO, Fe nanoparticles, and the ZnFeAl-LDH nanosheet precursor showed no activity for the CO hydrogenation. Fe₂O₃ and Fe₃O₄ nanosized reference materials showed modest CO conversions with high selectivities to CO₂ (72–86%) and almost negligible olefin/paraffin molar ratios (*o/p*) of 0.1 and 0.3, respectively (entries 5 and 6, Table 1; Figure S5, Supporting Information). Clearly, unsupported iron oxide nanoparticles are not desirable FT synthesis photocatalysts due to the high selectivity to CO₂, as noted previously by the Garcia group.^[12] The

Fe/Fe₃O₄ heterostructure formed via reduction in H₂ atmosphere (Figure S6, Supporting Information) afforded an olefin selectivity of 18.1% with *o/p* of ≈1.8 under light irradiation (entry 7, Table 1), clearly indicating metallic Fe is the active site for the formation of olefins in Fe/Fe₃O₄ heterostructured photocatalysts under light irradiation. Interestingly, Fe-350 showed a high CO₂ selectivity (60.2%). On increasing the LDH nanosheet reduction temperature (400 °C and above), metallic Fe nanoparticles gradually formed. Fe-500 displayed an excellent selectivity to olefins with an *o/p* ratio of 4.7 and an Anderson-Schulz-Flory (ASF) distribution growth factor (*a*) of 0.47 (Figure S7, Supporting Information). Importantly, Fe-500 showed a very low selectivity to CO₂ (only 11.4%). On increasing the ZnFeAl-LDH nanosheet precursor reduction temperature from 600 to 650 °C, the CO conversion dropped sharply from 20.7% to 8.4%, suggesting some unfavorable change in the electronic structure or morphology of the catalyst occurred during reduction at 650 °C. The selectivity to CO₂ increased progressively in the order Fe-500 (11.4%) < Fe-550 (16.3%) < Fe-600 (31.4%) ≈ Fe-650 (29.6%), whilst the *o/p* ratio decreased from 4.7 for Fe-500 to 2.6 for Fe-650. It is likely an increased Fe⁰:FeO_x ratio in the Fe-*x* photocatalysts caused this undesirable switch in product selectivity with increasing LDH precursor reduction temperature in the range 500–650 °C. Indeed, it would appear that there is an optimum Fe⁰ content in the Fe-*x* photocatalysts, best satisfied here by Fe-500. It should be mentioned that during conventional Fe-based FT processes used for alkene synthesis, selectivities to CO₂ typically fall in the range 23–50% (Table S1, Supporting Information). These values indicate a poor carbon resource utilization efficiency.^[11c,11a] Here,

Table 1. Performance comparison of various Fe-based photocatalysts for CO hydrogenation.^{a)}

Entry	Photo catalyst	CO Conversion [%]	Selectivity [%]					
			CO ₂	CH ₄	C ₂ –C ₄ olefin	C ₂ –C ₄ paraffin	C ₅₊	<i>o/p</i> ^{b)}
1	Blank ^{b)}	0	–	–	–	–	–	–
2	ZnO ^{c)}	0	–	–	–	–	–	–
3	Fe NPs ^{e)}	0	–	–	–	–	–	–
4	LDH	0	–	–	–	–	–	–
5	Fe ₂ O ₃ ^{d)}	54.6	72.0	11.1	1.1	12.9	2.9	0.1
6	Fe ₃ O ₄ ^{d)}	19.3	85.6	6.9	1.6	4.9	1.0	0.3
7	Fe/Fe ₃ O ₄ ^{f)}	10.1	40.0	18.2	18.1	10.3	13.4	1.8
8	Fe-350	7.2	60.2	12.6	19.4	3.3	4.5	5.9
9	Fe-400	24.0	37.2	24.0	18.8	14.8	5.2	1.3
10	Fe-450	20.3	14.9	22.6	39.5	8.0	15.0	4.9
11	Fe-500	20.9	11.4	28.6	42.4	9.0	8.6	4.7
12	Fe-550	27.5	16.3	25.8	32.9	13.5	11.5	2.4
13	Fe-600	20.7	31.4	25.5	27.5	9.6	6.0	2.9
14	Fe-650	8.4	29.6	16.0	22.7	8.7	23	2.6
15	Fe-500 ^{g)}	11.4	7.1	37.7	40.0	6.6	8.6	6.1
16	Fe-500 ^{h)}	12.0	18.4	20.9	41.6	7.9	11.2	5.3

^{a)}Reaction conditions: no external heating, 0.18 MPa, CO/H₂/N₂ = 20/60/20, catalyst mass: 100 mg, irradiation time: 2 h, 300 W Xe light (200–800 nm); ^{b)}Blank experiments, irradiation in the absence of any catalysts or illumination of the catalysts in Ar under above conditions; ^{c–e)}Commercially available reference materials; ^{f)}The synthesis of Fe/Fe₃O₄ catalyst was described in the Supporting Information; ^{g)}A flow system with the rate of 5 mL min⁻¹ under 300 W Xe irradiation after 20 h; ^{h)}Visible-light irradiation (420 < λ < 800 nm) for 4 h; ⁱ⁾The ratio of olefin to paraffin in C₂–C₄.

the Fe-500 photocatalyst showed a much lower selectivity to CO₂ (11.4%) and an optimal o/p ratio (4.7) under comparatively mild reaction conditions, with the majority of the CO converted being transformed into valuable C₂₊ hydrocarbons.

To confirm that the hydrocarbon products obtained under UV-vis irradiation of Fe-500 were from CO, further experiments were conducted using ¹³CO (Figure S8, Supporting Information). The experiments confirmed the activity of the Fe-x photocatalysts for CO activation and C–C coupling reactions. With increasing UV-vis irradiation time for 2–27 h, the CO conversion increased from 20.9% to 46.7%, though the selectivity to CO₂ increased from 11.4% to 26.5% along with a decrease in the o/p ratio (Table S2, Supporting Information). The decrease in the o/p is explained by the enhanced alkene hydrogenation, as noted in our previous work.^[5] The XRD patterns for the as-prepared and used Fe-500 (2 h) photocatalyst showed no obvious differences (Figure S9, Supporting Information). Further stability tests were conducted on Fe-500 (three successive cycles), during which the photocatalyst maintained good CO conversions with a low CO₂ selectivity (Figure S10A, Supporting Information). Further, the Fe-500 catalyst also displayed good selectivity (o/p 6.1) and stability over 20 h under UV-vis irradiation when tested under flow conditions (Figure S10B, Supporting Information; entry 15, Table 1) with a lower CO conversion of ≈11% being due to the short diffusion and contact time under flow conditions. The enhanced o/p ratio (6.1) in flow reactor can be understood by the quick desorption of the olefins, that avoiding the over hydrogenation to paraffin compared with the batch reactor.

Of particular interest was the operating mechanism of Fe-500 for CO hydrogenation, which could possibly have been due to either photocatalytic or photothermal mechanisms. Under UV-vis irradiation, the temperature of the Fe-500 catalyst bed increased rapidly from 23 to 230 °C over a period of ≈25 min, after which the temperature remained constant (Figure S4B,C, Supporting Information). Such a low temperature for CO activation shown by Fe-500 is rare amongst Fe-based FT catalysts, which generally require temperatures above 300 °C and high pressures (2.0 MPa) to achieve meaningful CO conversions (Table S1, Supporting Information). To confirm the photocatalytic activity of Fe-500, a control experiment was conducted using external heating and no UV-vis irradiation (with all other reaction conditions kept the same). The control experiment showed a lower CO conversion (9.9%), with high selectivity to CO₂ (60.8%) and CH₄ (52.3% in hydrocarbons) (Table S3, Supporting Information). Thus, it can be concluded that the high selectivity of Fe-500 for CO hydrogenation to olefins is primarily due to a photocatalytic pathway, with photothermal effects enhancing CO conversion though not product selectivity to C₂₊ hydrocarbons, including olefins. The mechanism of olefins synthesis via photocatalysis is discussed below. Furthermore, under visible-light irradiation (the catalyst-bed temperature was around 225 °C), Fe-500 catalysts also displayed good performance for photocatalytic FT reaction (entry 16, Table 1), with a low CO₂ selectivity of 18.4% and a good o/p ratio (5.3). Since the Zn-oxide is a UV-responsive semiconductor (and thus should be inactive under visible light), the visible-light-driven photocatalytic FT synthesis performance of Fe-500 strongly suggested that the heterostructured Fe/FeO_x in

Fe-500 played an important role in the olefins synthesis under light (visible-light) irradiation, while Zn and Al oxides in Fe-500 mainly act as a structural support. The lower CO conversion achieved under visible-light excitation compared with UV-vis excitation can be rationalized in terms of the lower energy input in the former case. Electron spin resonance (ESR) provided further supporting evidence for a photocatalytic pathway, where hydroxyl radicals and superoxide radicals (formed from reactions involving photoexcited holes and electrons, respectively) were detected from Fe-500 under light excitation (Figure S11, Supporting Information). The data add support to the hypothesis that the FT reaction on Fe-500 involves photocatalytic processes.

The structural evolution of Fe-x during the LDH precursor reduction process at temperature between 300 and 650 °C was thus of particular importance in CO hydrogenation to hydrocarbons. In particular, Fe-500 offered an optimal platform for CO hydrogenation with a good o/p ratio and low CO₂ selectivity. If the reduction temperature is too low (<400 °C), no Fe⁰ is formed and the photocatalyst performance was poor. If the reduction temperature is too high (>600 °C), too much Fe⁰ is formed, which also detrimentally impacted performance. It is therefore intuitive that there must be an optimal amount of metallic Fe in the ZnFeAl-LDH derived catalysts which serves as the active site for CO hydrogenation, with the coexistence of abundant interfaces of Fe and FeO_x, providing a heterostructured photocatalyst system with moderate intermediate binding energies (for intermediates like –CH₂ and its coupling products), thereby promoting alkene formation and suppressing CO₂ evolution.

Fe K-edge X-ray absorption near-edge spectroscopy (XANES) and extended X-ray absorption fine structure (EXAFS) were used to probe the local coordination of iron in Fe-x photocatalysts (Figure 1C,D). The Fe K-edge XANES spectra for Fe-x reduced below 400 °C were similar to those of the Fe oxide reference materials, indicating that FeO_x was the dominant iron-containing state in these photocatalysts. For Fe-400, Fe-500, and Fe-650, an additional feature was observed on the low photon energy side of the FeO_x peaks, which could be readily assigned to metallic Fe. The Fe⁰ feature intensified with reduction temperature, in accordance with the XRD data (Figure 1A). The Fe K-edge XANES analyses provide strong evidence for the coexistence of Fe and FeO_x in Fe-x ($x > 400$). In case of Fe-650, Fe⁰ was the dominant Fe species. EXAFS at the Fe K-edge results showed the appearance of a weak Fe–Fe peak (indicating metallic Fe) at around 2.2 Å for Fe-400, which increased in intensity for Fe-500 and Fe-650 at the expense of peaks due to Fe oxides (Fe–O at 1.5 Å and Fe–Fe around 2.8 Å). Zn K-edge XANES and Zn K-edge EXAFS results (Figure S12, Supporting Information) revealed that Zn in Fe-x existed mainly as zinc-oxide.

Since CO hydrogenation occurs on the surface of the Fe-x photocatalysts, a detailed investigation of their surface chemical composition was undertaken. Figure 1E,F and Figure S13 (Supporting Information) show *in situ* X-ray photoelectron spectroscopy (XPS) data collected from the Fe 2p and Zn 2p regions during reduction of the ZnFeAl-LDH nanosheet precursor in H₂ at 300–650 °C. The binding energy scale was calibrated against the C 1s signal at 284.8 eV. The Fe 2p XPS spectrum for

Fe-300 contained signals and shake-up satellites characteristic for Fe^{2+} and Fe^{3+} (Figure 1E), consistent with the presence of Fe oxides (in accord with ex situ XRD and EXAFS analyses). On increasing the reduction temperature, metallic Fe peaks appear on the low binding energy side of the oxide-related signals. Fe-500 showed the most intense Fe^0 signals. Interestingly, when the reduction temperature was increased further to 650 °C, the intensity ratio $\text{Fe}^0/\text{Fe}_{\text{ox}}$ progressively decreased, whilst the Fe 2p peak positions for the Fe^0 species also exhibited a small shift to lower binding energies. The decreased amount of active metallic Fe^0 sites in Fe-650 explains the suppressed CO conversion (~8.4%) relative to Fe-500 (20.9%). Simultaneously, the Zn 2p peaks for the Fe- x catalysts also shifted to lower binding energy when the reduction was higher than 500 °C (Figure 1F). XRD and EXAFS results confirmed that the amount of metallic Fe in the Fe- x photocatalysts increased with reduction temperature above 400 °C. Thus, we attribute the apparent decrease in metallic Fe for Fe- x ($x > 500$) to a progressive formation of FeZn alloy, which modifies slightly the electronic properties of Fe^0 and ZnO , thus accounting for the small binding energy shifts seen by XPS at the higher reduction temperatures. XPS depth analysis experiments provided support to this hypothesis, where the ratios $\text{Fe}^0/\text{Fe}_{\text{total}}$ and $\text{Fe}^0/(\text{Fe}_{\text{total}} + \text{Zn})$ increased with analysis depth (Figure S14, Supporting Information). Metallic

Zn formed at high reduction temperatures, giving rise to an FeZn alloy (Figure S12B, Supporting Information). The formation of such alloys was also reported by the Schlägl group during the reduction of CuZnAl-LDH at high temperatures.^[13] No clear evidence could be found for FeZn alloy formation by XRD, suggesting that it was a very minor component, even in the Fe-650 photocatalyst. The observation that the Fe-500 photocatalyst had the highest surface concentration of Fe^0 amongst the Fe- x photocatalysts prepared in this study has important implications, since Fe-500 displayed the best performance for CO hydrogenation to olefins, with the lowest product selectivity to CO_2 . The important role of surface metallic Fe phase to the performance of the Fe- x is firmly established.

^{57}Fe Mössbauer spectroscopy was also used to track the transformation of Fe during the photocatalytic FT reaction. The ^{57}Fe Mössbauer spectra and XRD data showed that metallic Fe and FeO_x coexisted in Fe-500 (Figures S9, S15 and Table S4, Supporting Information) during the first 2 h of the reaction. Thus, it is very likely that metallic Fe acts as the main active species for CO hydrogenation, with the supporting oxide phases (FeO_x and ZnO) acting as photoactive elements and also electronic and structural promoters. All of the above structural features result in the activation of CO and its hydrogenation to olefins, along with the suppression of CO_2 formation.

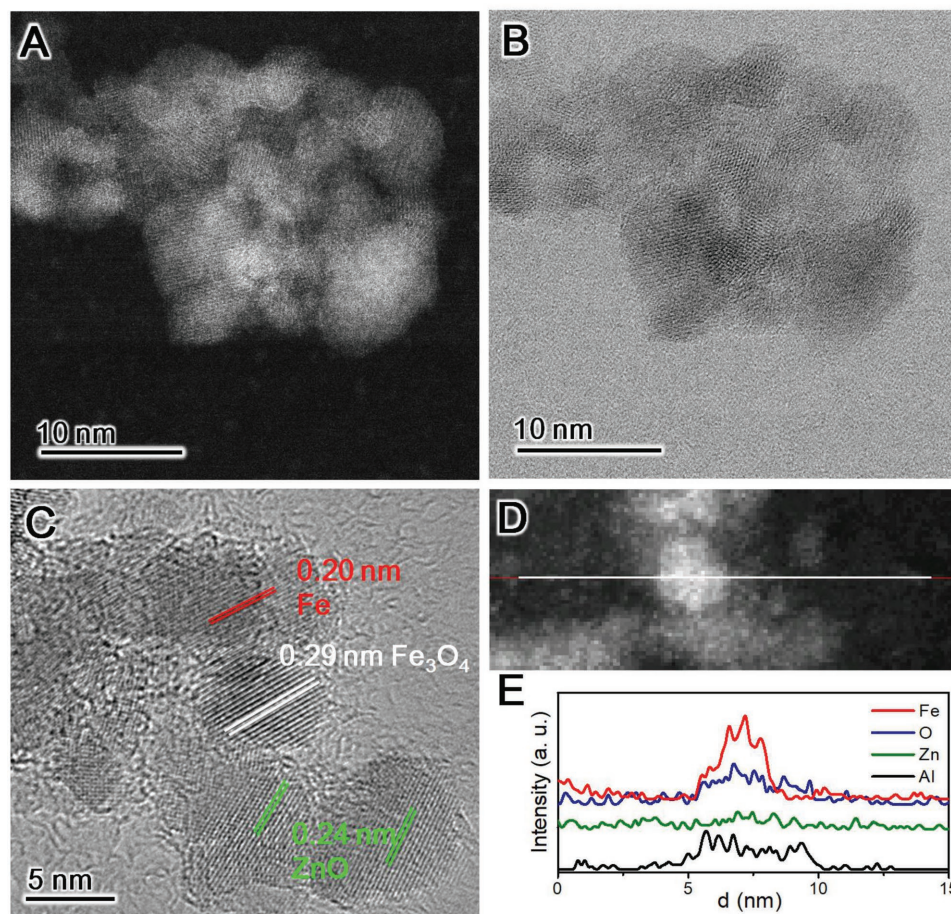


Figure 2. A,B) High-angle annular dark-field scanning TEM (HAADF-STEM) image and C) high-resolution TEM (HRTEM) image of Fe-500. D) STEM image of one Fe particle, and E) the corresponding element (Fe, O, Zn, Al) intensity line-scan profiles.

A detailed transmission electron microscopy (TEM) investigation was undertaken to try to identify the distinct phases and heterojunctions present in the Fe-500 photocatalyst. During reduction of the LDH nanosheet precursor, Fe_2O_3 and ZnO phases formed at around 350 °C (i.e., in Fe-350), and metallic Fe evolved when the reduction temperature was increased to 400 °C or higher (Figure S3, Supporting Information). Compared with the nanostructured ZnO and Fe_2O_3 heterojunction obtained from Fe-MMO (Figure S16, Supporting Information), Fe-500 showed a very close association of Fe^0 , FeO_x , and ZnO nanoparticles (Figure 2) with metallic Fe nanoparticles of size ≈ 5 nm confirmed by the energy dispersive spectroscopy (EDS) line scan (Figure 2E), all supported to some degree by alumina. TEM data for Fe-550 and Fe-600 were similar to Fe-500 (Figure S17, Supporting Information), whereas for Fe-650, some FeAl_2O_4 spinel phases were formed due to the high reduction temperature (Figure S18, Supporting Information).

In order to understand the activity and selectivity patterns of the difference in $\text{Fe}-x$ photocatalysts for CO hydrogenation under UV-vis excitation, constrained density functional theory (DFT) calculations^[14] were performed to simulate the photocatalysis on Fe_3O_4 , 4O/Fe, and 4O/ Fe_3Zn alloy surfaces to represent $\text{Fe}-x$ catalysts prepared at low (350 °C), moderate (500 °C), and high (>500 °C) reduction temperatures, respectively. The calculation models (Figure S19, Supporting Information) and computational details are provided in the Supporting Information. In the FT reaction, it is usually accepted that CO_2 is derived from the WGS reaction.^[15] The elementary reaction $\text{CO} + \text{OH} \rightarrow \text{COOH}$ is considered as the rate-determining step. Thus, the formation of COOH and CO_2 on each of the different representative catalyst surfaces under photoexcitation was investigated. Figure 3A and Figure S20A (Supporting Information) show that the formation of COOH is exothermic on Fe_3O_4 (-0.83 eV), and endothermic on 4O/Fe (1.52 eV) and 4O/ Fe_3Zn (1.13 eV). For CO_2 formation, it is exothermic 0.11 eV on the Fe_3O_4 and 0.42 eV on the 4O/ Fe_3Zn , while it is endothermic on the 4O/Fe (0.15 eV). From a thermodynamics perspective, COOH and CO_2 formation on Fe_3O_4 are much easier than either 4O/Fe or 4O/ Fe_3Zn . The fact that COOH and CO_2 formation required significant energy input on the 4O/Fe catalyst agrees well with Fe being the proposed active site in the Fe-500 (the photocatalyst which displayed the lowest selectivity to CO_2).

To understand the difference in olefin selectivity between the Fe-350, Fe-500, and Fe-650, the adsorption and hydrogenation of ethene on three surface models were calculated (Figure 3A; Figure S20B, Supporting Information). The adsorption energies were found to be similar (-1.24 eV on the Fe_3O_4 ; -1.31 eV on the 4O/Fe; -1.19 eV on the 4O/ Fe_3Zn), indicating that the interaction between ethene and the three surface models is comparable. However, for ethene hydrogenation, it is exothermic 1.34 eV on Fe_3O_4 . On 4O/ Fe_3Zn , the transformation of C_2H_4 to C_2H_5 is endothermic (0.32 eV) and C_2H_5 to ethane exothermic (0.09 eV). It should be noted that on the 4O/Fe model (i.e., Fe-500), both elementary steps are endothermic (0.53 eV and 0.54 eV for $\text{C}_2\text{H}_4 \rightarrow \text{C}_2\text{H}_5$ and $\text{C}_2\text{H}_5 \rightarrow \text{C}_2\text{H}_6$, respectively). Thus for the Fe_3O_4 (i.e., Fe-350) and the 4O/ Fe_3Zn (i.e., Fe-650) surfaces, the hydrogenation of ethene requires less energy input, resulting in ethene over hydrogenation to alkanes, which dominates the reaction products and leads to lower olefins

selectivity. For the 4O/Fe surface (i.e., Fe-500), the hydrogenation of ethene needs significant energy input, whilst the desorption of ethene is energetically favorable, leading to a significant increase in olefin selectivity, explaining the high o/p (4.7) of Fe-500 under light irradiation.

To further clarify mechanistic differences between thermal-driven and photo-driven catalysis, CO_2 formation and the adsorption and hydrogenation of ethene under the ground state (thermal catalysis) and excited state (photocatalysis) regimes were simulated on the 4O/Fe surface model, as shown in Figure 3B and Figure S21 (Supporting Information). It is obvious that CO_2 formation under the ground state conditions requires less energy input than the excited state (1.35 vs 1.52 eV for $\text{CO} + \text{OH} \rightarrow \text{COOH}$ and 0.01 vs 0.15 eV for $\text{COOH} \rightarrow \text{CO}_2 + \text{H}$). However, for ethene adsorption and hydrogenation, ethene interacts more strongly with surface under the excited state conditions (1.31 vs 1.01 eV), with further hydrogenation demanding more energy input (0.53 vs 0.30 eV and 0.54 vs 0.21 eV for $\text{C}_2\text{H}_4 \rightarrow \text{C}_2\text{H}_5$ and $\text{C}_2\text{H}_5 \rightarrow \text{C}_2\text{H}_6$, respectively). The results indicate the advantage of the photocatalysis pathway in achieving a low CO_2 selectivity (11.4%) and high

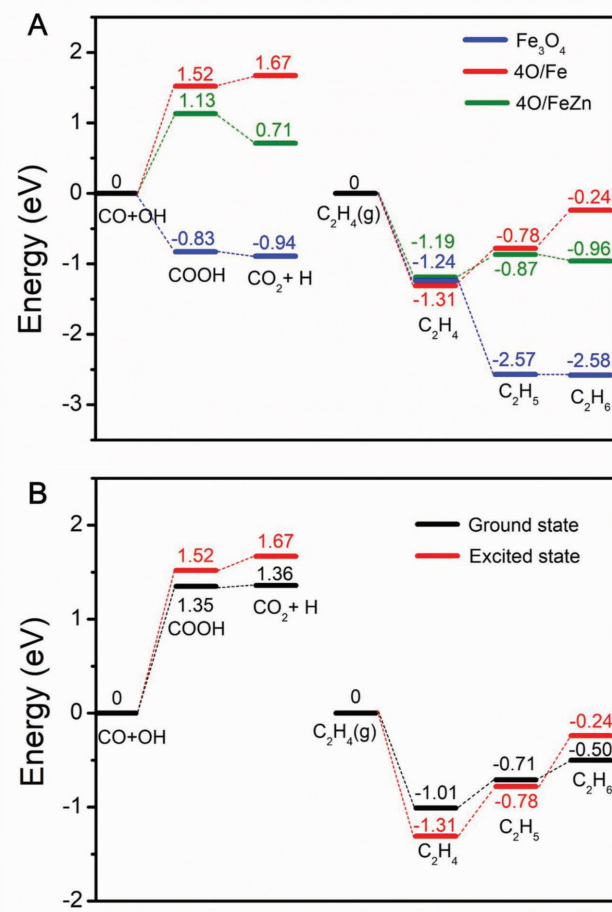


Figure 3. The potential energy profiles for CO_2 formation, C_2H_4 adsorption, and hydrogenation under: A) excited states on Fe_3O_4 , 4O/Fe, and 4O/ Fe_3Zn , and B) ground states and excited states (thermal- and photo-driven catalysis) on 4O/Fe.

ethene selectivity (47.8% olefins in hydrocarbons) compared with ground state thermal catalysis processes (60.8% for CO₂, 37.2% olefins in hydrocarbons), as summarized in Table S3 (Supporting Information).

In summary, through controlled reduction of ZnFeAl-LDH nanosheets at 500 °C, an Fe-based heterostructured photocatalyst was obtained that displayed remarkably high selectivity for alkenes, with suppressed WGS activity to CO₂, during the FT reaction under both UV-vis and visible irradiation. Detailed *in situ* characterization experiments show that the heterostructured Fe-500 photocatalysts comprising Fe and FeO_x supported on zinc-oxide and alumina, which afforded a near-perfect surface electronic structure for the photocatalytic FT reaction. DFT calculations suggested that the formation of interfaces between Fe and the oxides tuned the product selectivity towards olefins and suppressed CO₂ evolution under photoirradiation. This work offers a new pathway for synthesis of olefins that uses Fe-based nanostructured photocatalysts in CO hydrogenation. Further research on other FT active phases (such as CoC_x, CoN, and FeCo alloy structures) for the solar-driven CO hydrogenation is currently underway.

Supporting Information

Supporting Information is available from the Wiley Online Library or from the author.

Acknowledgements

Y.Z., Z.L., and M.L. contributed equally to this work. The authors are grateful for the financial support from the National Key R&D Program of China (2016YFB0600901, 2017YFA0206904, 2017YFA0206900, 2017YFB0602200), the National Basic Research Program of China (2014CB239402), the National Natural Science Foundation of China (51772305, 51572270, U1662118, 31671489, 51861135101, 21725301, 91645115, 21673273, 21473229, 91545121), the Strategic Priority Research Program of the Chinese Academy of Sciences (XDB17000000), the Royal Society-Newton Advanced Fellowship (NA170422), the International Partnership Program of Chinese Academy of Sciences (GJHZ1819), the Young Elite Scientist Sponsorship Program by CAST (YES20160137) and the Youth Innovation Promotion Association of the CAS, National Thousand Young Talents Program of China, the Hundred-Talent Program of Chinese Academy of Sciences, the Shanxi Hundred-Talent Program, The XAFS experiments were conducted in 1W1B beamline of Beijing Synchrotron Radiation Facility (BSRF).

Conflict of Interest

The authors declare no conflict of interest.

Keywords

CO hydrogenation, Fe-based catalysts, layered double hydroxides, light olefins, photocatalysis

Received: May 16, 2018

Revised: June 20, 2018

Published online: July 31, 2018

- [1] a) H. M. T. Galvis, J. H. Bitter, C. B. Khare, M. Ruitenberg, A. I. Dugulan, K. P. de Jong, *Science* **2012**, *335*, 835; b) A. Y. Khodakov, W. Chu, P. Fongarland, *Chem. Rev.* **2007**, *107*, 1692; c) L. Zhong, F. Yu, Y. An, Y. Zhao, Y. Sun, Z. Li, T. Lin, Y. Lin, X. Qi, Y. Dai, L. Gu, J. Hu, S. Jin, Q. Shen, H. Wang, *Nature* **2016**, *538*, 84.
- [2] a) F. Jiao, J. Li, X. Pan, J. Xiao, H. Li, H. Ma, M. Wei, Y. Pan, Z. Zhou, M. Li, S. Miao, J. Li, Y. Zhu, D. Xiao, T. He, J. Yang, F. Qi, Q. Fu, X. Bao, *Science* **2016**, *351*, 1065; b) K. Cheng, B. Gu, X. Liu, J. Kang, Q. Zhang, Y. Wang, *Angew. Chem., Int. Ed.* **2016**, *55*, 4725; c) J. Xie, J. Yang, A. I. Dugulan, A. Holmen, D. Chen, K. P. de Jong, M. J. Louwerse, *ACS Catal.* **2016**, *6*, 3147.
- [3] K. Xu, B. Sun, J. Lin, W. Wen, Y. Pei, S. R. Yan, M. H. Qiao, X. X. Zhang, B. N. Zong, *Nat. Commun.* **2014**, *5*, 8.
- [4] a) S. S. K. Ma, T. Hisatomi, K. Maeda, Y. Moriya, K. Domen, *J. Am. Chem. Soc.* **2012**, *134*, 19993; b) S. J. A. Moniz, S. A. Shevlin, D. J. Martin, Z.-X. Guo, J. Tang, *Energy Environ. Sci.* **2015**, *8*, 731; c) C. Gomes Silva, Y. Bouizi, V. Fornes, H. Garcia, *J. Am. Chem. Soc.* **2009**, *131*, 13833; d) X. Guo, Z. Jiao, G. Jin, X. Guo, *ACS Catal.* **2015**, *5*, 3836; e) F. Sastre, A. V. Puga, L. Liu, A. Corma, H. Garcia, *J. Am. Chem. Soc.* **2014**, *136*, 6798; f) K. K. Ghuman, L. B. Hoch, P. Szymanski, J. Y. Y. Loh, N. P. Kherani, M. A. El-Sayed, G. A. Ozin, C. V. Singh, *J. Am. Chem. Soc.* **2016**, *138*, 1206; g) L. Wang, M. Ghoussoob, H. Wang, Y. Shao, W. Sun, A. A. Tountas, T. E. Wood, H. Li, J. Y. Y. Loh, Y. Dong, M. Xia, Y. Li, S. Wang, J. Jia, C. Qiu, C. Qian, N. P. Kherani, L. He, X. Zhang, G. A. Ozin, *Joule* **2018**, *2*, 1369; h) S. Wang, X. Hai, X. Ding, K. Chang, Y. Xiang, X. Meng, Z. Yang, H. Chen, J. Ye, *Adv. Mater.* **2017**, *29*, 1701774; i) X. Meng, L. Liu, S. Ouyang, H. Xu, D. Wang, N. Zhao, J. Ye, *Adv. Mater.* **2016**, *28*, 6781; j) Y. Izumi, *Coord. Chem. Rev.* **2013**, *257*, 171; k) J. L. Gunjakar, T. W. Kim, H. N. Kim, I. Y. Kim, S. J. Hwang, *J. Am. Chem. Soc.* **2011**, *133*, 14998.
- [5] Y. Zhao, B. Zhao, J. Liu, G. Chen, R. Gao, S. Yao, M. Li, Q. Zhang, L. Gu, J. Xie, X. Wen, L. Z. Wu, C. H. Tung, D. Ma, T. Zhang, *Angew. Chem., Int. Ed.* **2016**, *55*, 4215.
- [6] a) J. Feng, Y. He, Y. Liu, Y. Du, D. Li, *Chem. Soc. Rev.* **2015**, *44*, 5291; b) G. Fan, F. Li, D. G. Evans, X. Duan, *Chem. Soc. Rev.* **2014**, *43*, 7040; c) M. Xu, S. He, H. Chen, G. Cui, L. Zheng, B. Wang, M. Wei, *ACS Catal.* **2017**, *7*, 7600; d) R. Ma, T. Sasaki, *Acc. Chem. Res.* **2015**, *48*, 136; e) Z. Pan, Y. Jiang, P. Yang, Z. Wu, W. Tian, L. Liu, Y. Song, Q. Gu, D. Sun, L. Hu, *ACS Nano* **2018**, *12*, 2968.
- [7] Q. Zhang, J. Kang, Y. Wang, *ChemCatChem* **2010**, *2*, 1030.
- [8] B. C. Enger, A. Holmen, *Catal. Rev.: Sci. Eng.* **2012**, *54*, 437.
- [9] L. Zhang, F. Li, X. Xiang, M. Wei, D. G. Evans, *Chem. Eng. J.* **2009**, *155*, 474.
- [10] a) M.-Q. Zhao, Q. Zhang, W. Zhang, J.-Q. Huang, Y. Zhang, D. S. Su, F. Wei, *J. Am. Chem. Soc.* **2010**, *132*, 14739; b) G.-L. Tian, M.-Q. Zhao, B. Zhang, Q. Zhang, W. Zhang, J.-Q. Huang, T.-C. Chen, W.-Z. Qian, D. S. Su, F. Wei, *J. Mater. Chem. A* **2014**, *2*, 1686.
- [11] a) P. Zhai, C. Xu, R. Gao, X. Liu, M. Li, W. Li, X. Fu, C. Jia, J. Xie, M. Zhao, X. Wang, Y.-W. Li, Q. Zhang, X.-D. Wen, D. Ma, *Angew. Chem., Int. Ed.* **2016**, *55*, 9902; b) S. Li, A. Li, S. Krishnamoorthy, E. Iglesia, *Catal. Lett.* **2001**, *77*, 197.
- [12] F. Sastre, A. Corma, H. Garcia, *Angew. Chem., Int. Ed.* **2013**, *52*, 12983.
- [13] M. Behrens, F. Studt, I. Kasatkin, S. Kuehl, M. Haevecker, F. Abild-Pedersen, S. Zander, F. Girsachs, P. Kurr, B.-L. Kniep, M. Tovar, R. W. Fischer, J. K. Norskov, R. Schloegl, *Science* **2012**, *336*, 893.
- [14] P. H. Dederichs, S. Blügel, R. Zeller, H. Akai, *Phys. Rev. Lett.* **1984**, *53*, 2512.
- [15] Z.-J. Zhao, Z. Li, Y. Cui, H. Zhu, W. F. Schneider, W. N. Delgass, F. Ribeiro, J. Greeley, *J. Catal.* **2017**, *345*, 157.